Computational Model of Nano-Pharmacological Particles for the Clinical Management of Stenotic and Aneurysmatic Coronary Artery in the Human Body

I. A. Fetuga*, O. O. Olakoyejo, O. Oluwatusin, A. O. Adelaja, J. K. Gbegudu, K. S. Aderemi, E. A. Adeyemi

Department of Mechanical Engineering, University of Lagos, Akoka, Lagos, Nigeria.

ABSTRACT: This work presents a three-dimensional computational study of nanoparticles (metallic and non-metallic) suspended in blood flowing through a diseased artery with both stenosis and aneurysm. From the perspective of pharmacodynamics and heat transfer, the influence of nanoparticles on hemodynamic indicators was investigated in a diseased artery. The blood was flowing fluid, steady-state, incompressible, homogeneous, and Newtonian, while the artery was a rigid wall. The three-dimensional continuity, Navier-Stokes, and energy equations were solved numerically by using a RAN-based standard k-ω model, which was performed on the ANSYS commercial software package. The influence of different selected nanoparticles (Al_2O_3, CuO, SiO_2, and ZnO), nanoparticle concentration (1.0%-4.0%), and nanoparticle diameters (25 nm - 100 nm) on hemodynamic parameters such as velocity, temperature, turbulence intensity, more particularly skin friction coefficient and Nusselt number of the blood flow on the diseased artery, was also investigated. The streamlines, contours, and plots were adopted to better visualize the blood flow behavior in an artery with stenosis and aneurysm. The numerical results revealed that at a 4.0% nanoparticle concentration, CuO nanoparticles greatly reduced the blood velocity by 1.96% compared to other nanoparticles. About 0.66%-2.05% reduction in the blood velocity could be achieved by increasing the nanoparticle concentration from 1.0% to 4.0%. The SiO_2 blood nanofluid showed the best result in augmentation of the Nusselt number by 53.0%. However, the nanoparticle diameter and concentration showed an insignificant effect on the skin friction factor.

KEYWORDS: Stenosis, Aneurysm, Nanoparticles, Nusselt number, Skin friction coefficient

[Received Aug. 8, 2022; Revised Nov. 23, 2022; Accepted Jam. 13, 2023] Print ISSN: 0189-9546 | Online ISSN: 2437-2110

I. INTRODUCTION

An abnormal change in the number of cells of the blood vessel causes arterial diseases in different organs of the cardiovascular system of the human body. Stenosis is a result of an arterial disease called atherosclerosis that reduces the area of the lumen, and this obstructs the blood flow in the lumen of an artery. An aneurysm is a weakening and abnormally large bulge in the arterial wall. The bulge can further rupture and cause internal bleeding, which mostly occurs in the aorta, brain, and spleen. Aortic aneurysms cause approximately 13,000 deaths annually in the United States (Kent, 2014).

Over the years, scientists and medical engineers have developed a keen interest in this area by extensively carrying out studies and research on arterial diseases. Nanofluids were first proposed by (Choi *et al*., 2001) at Argonne National Laboratory. Choi employed the nanoparticles as a suspended solution. The study found that the nanofluid thermal conductivity significantly increased. (Choi, Li and Eastman, 1999) measured the thermal conductivity of nanofluid. The results found that a suspension containing 4.0% of 35 nm CuO particles in ethylene glycol had an increment of 20% in the thermal conductivity. (Nadeem and Ijaz, 2015) theoretically analyzed the metallic nanoparticles in blood flow through tapered, curved arteries. The study revealed that the curvature of the curved arteries was dominated by stenosis. (Mekheimer, Haroun and El Kot, 2011) examined the blood flow under the influence of an induced magnetic field through an anisotropically tapered elastic artery with overlapping stenosis (Keith L. Moore, Agur Moore and Anne M.R. Agur, 2009) suggested that it was better to investigate the blood flow of an artery with post-stenotic dilation because multiple stenoses with post-stenotic dilatations, and aneurysms, commonly occur in coronary arteries. (Ellahi *et al*., 2014) studied non-Newtonian micropolar fluid by using Eringen's model in the blood flow through composite stenosis. The study was further extended by investigating the influence of nanoparticles suspended in blood fluid flowing through the composite arterial stenosis with permeable walls. (Bluestein *et al*., 1996) experimentally and numerically studied both laminar and turbulence flow in an aneurysmatic artery. From their results, it was found that a recirculation zone was formed downstream of the aneurysm cavity and that it could induce the formation of the thrombus as a result of the arterial wall rupture. (Karimi *et al*., 2013) reported the effects of rheology on hemodynamic parameters by considering blood as non-Newtonian Carreau

*Corresponding author: fetugaebraheem@gmail.com

doi: http://dx.doi.org/10.4314/njtd.v20i1.1293

and modified power-law fluid through a stenotic carotid artery. (Karimi *et al.*, 2016) further discussed the application of nanotechnologies, such as nano-coatings and nano-carriers, as a tool for the treatment and diagnosis of arterial diseases. In the quest to cultivate atherosclerotic plaque. (Rhee and Wu, 2013) reported that nano-carriers are effective tools for diagnosis and image delivery of arterial disease. (Mandal *et al*., 2022) computationally studied the influence of symmetrical and asymmetrical bell-shaped stenosis on blood flow characteristics under the steady state and pulsatile conditions. The study showed that the asymmetrical bell-shaped stenosis greatly influenced hemodynamics indicators than the symmetrical form of stenosis. (Ul Haq *et al*., 2022) employed a fluid-structure interaction method to conduct a simulation on stenotic cerebral aqueduct resulting from brain tumour. The study reported a steeply rise in velocity from 21.2mm/s at the pre-stenotic area to 54.1mm/s at the throat of the stenosis. (Yi *et al*., 2022) investigated the impact of surface roughness in a stenotic artery. The study revealed that the roughness in the stenotic site induced the oscillatory flow at the area distal to the stenosis and the effect of roughness on pressure distribution is very insignificant as compared to smooth wall artery. (Gosman *et al*., 2022) studied the airflow dynamics of drug delivery in one and two-level laryngotracheal stenosis. The study reported an increased airflow resistance at the stenotic area of the two-level stenosis. (Frank-Ito and Cohen, 2021) performed a simulation on an orally drug-delivery particles in a laryngotracheal stenosis at inlet pressure of 10Pa-40Pa and particle sizes of 1-50 um and 100-950um. The study reported 2.6% deposition of the inhaled drug particles at the stenotic site. (Waqas *et al*., 2022) numerically investigated magnetohydrodynamic behavior of the gold and silver nanofluid in a stenotic artery. The study found that the temperature and velocity decreased as the size of the gold and silver nanoparticles increased.

The advent of pharmaceutical agents that can cross the blood-brain barrier holds considerable promise for the nanotechnology in the field of pharmacotherapy. Despite the numerous research on aneurysm and stenosis in recent years, it is very unfortunate that the published work on application of nanotechnologies to diseased artery with both aneurysm and stenosis is very scarce. It is evident that no researcher has made an attempt to investigate the thermal and hemodynamic characteristics of Al_2O_3, CuO, SiO_2, and ZnO drug delivery nanoparticles in an artery with combined aneurysm and stenosis stenotic artery. Thus, it is very important to clinically manage this coronary artery disease (CAD) disease. Therefore, there is need to examine the hydrothermal influence of nano-pharmacological particles on the coronary artery consisting of both aneurysm and stenosis. The main objective of the present work is to investigate the hydrothermal influence of both metallic and non-metallic nanoparticles suspended in blood flowing through the artery with both stenosis and aneurysm. ANSYS Fluent commercial software package was used to perform three-dimension numerical simulations on steno-aneurysmatic coronary artery with blood flow consisting of Al_2O_3, CuO, SiO_2, and ZnO nanoparticles at Reynolds number ranging from 200 to 500. This research will catch the attention of many readers engaged in the fields of bioscience, pharmacology, nanotechnology, and medical engineering.

II. METHODOLOGY

A. Geometry Description

The geometry was created using the Design Modeler component of the ANSYS fluent software. It is considered a 3D incompressible (viscous) and steady nano-hemodynamic fluid flowing through an artery of finite length L with a rigid wall that contains a cosine-shaped aneurysm and stenosis. Blood is taken as Newtonian, a non-homogeneous fluid containing uniform nanoparticles. The continuity, Navier Stoke, and energy equations for incompressible viscous fluid and the steady nano-hemodynamic fluid flow have been considered for the solution of axial and radial velocities and pressure (p). Using the geometry configuration in Figure 1 through 3, the cylindrical polar coordinates system (r, θ, z) is used to indicate the point in the domain where r, θ, z represents radial, circumferential, and axial direction respectively. More so, heat transfer behavior is taken into consideration by temperature given as T_w assigned to the wall of the artery. In the artery, the physical configuration of the stenosis and aneurysm in the gaussian profile is defined mathematically as:

$$(z) = \begin{cases} 0.5D_i\left[1 - \frac{h_s}{D_i}\left(1 + cos\pi\left(z - \frac{z_s}{L_i}\right)\right)\right]; 0 \le z \le L_s\ (stenosis) \\ 0.5D_i\left[1 + \frac{h_a}{D_i}\left(1 + cos\pi\left(z - \frac{z_a}{L_i}\right)\right)\right]; 0 \le z \le L_a\ (aneurysm) \\ 1 \qquad\qquad\qquad\qquad\qquad ;\ otherwise \end{cases} \tag{1}$$

where z_s, and z_a defines the center of the stenosis and aneurysm, h_s and h_a which represent the maximum height of the stenosis and aneurysm are the same in value, D_i is the diameter of the artery of the i^{th} abnormal segment, R is the radius of the artery L_s and L_a are the length of stenosis and aneurysm, respectively. L_i is the finite length of the artery; stenosis is located at a distance L_d from the inlet of the artery while the aneurysm is positioned at a distance L_m from the downstream of the stenosis. Meanwhile, blood flows in the z-axis direction and is normal to the r- axis (See Table 1 for the details of the geometry).

B. Problem Formulation

The governing equations and boundary conditions (see Table 4) used in the problem are described in this section.

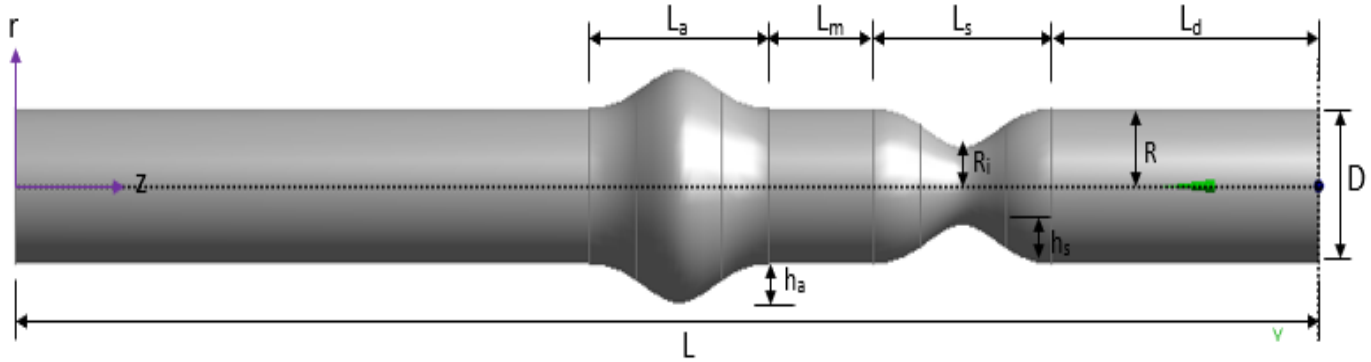

Figure 1. 2D Geometry of the artery with both stenosis and aneurysm

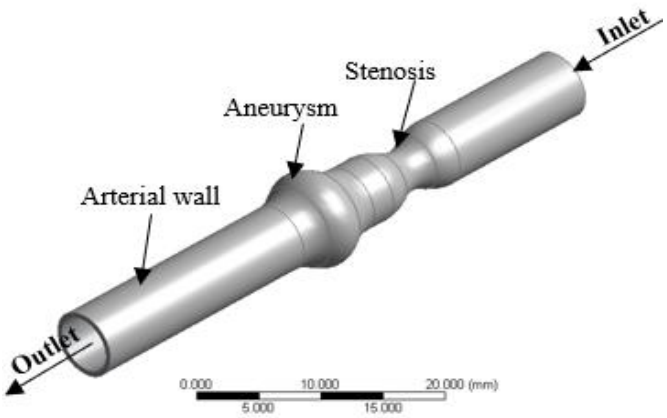

Figure 2. 3D view of the geometry

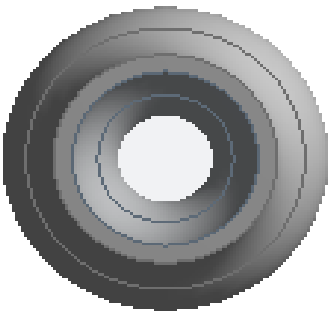

Figure 3. End view of the geometry

Table 1 Dimension details of the geometry

Parameter	Dimension
L	11D
R	D/2
R_i	0.75D
h_s	0.25D
h_a	0.25D
L_s	1D
L_a	1D
L_m	1.4D
L_d	2D

Navier-Stokes, continuity equations, and energy equation coupling with the two-equation low Reynold number k-ω turbulent model are adopted to solve the problem in this study. To properly formulate the computational domain for the coronary artery with stenosis and aneurysm, the problem is simplified by the following imposed assumptions:

1. The flow is 3D incompressible and steady state.
2. The fraction of red blood cell diameter to the diameter of the large artery is very small. Therefore, it is considered negligible.
3. The blood flow is considered to be Newtonian because non-Newtonian is revealed to exist in the smaller vessels such as capillaries.
4. The artery is assumed to be a rigid wall.
5. A no-slip condition is assigned to the solid-fluid interface.

The governing equations for the continuity, momentum, and energy equation in terms of nanofluid are as follows:

$$\frac{\partial \bar{u}}{\partial \bar{r}} + \frac{\bar{u}}{\bar{r}} + \frac{\partial \bar{w}}{\partial \bar{z}} = 0 \quad (2)$$

$$\rho_{nf}\left(\bar{u}\frac{\partial \bar{u}}{\partial \bar{r}} + \bar{w}\frac{\partial \bar{u}}{\partial \bar{z}}\right) = -\frac{\partial \bar{P}}{\partial \bar{r}} + \mu_{nf}\left(\frac{\partial^2 \bar{u}}{\partial \bar{r}^2} + \frac{1}{\bar{r}}\frac{\partial \bar{u}}{\partial \bar{r}} + \frac{\partial^2 \bar{u}}{\partial \bar{z}^2}\right) \quad (3)$$

$$\rho_{nf}\left(\bar{u}\frac{\partial \bar{w}}{\partial \bar{r}} + \bar{w}\frac{\partial \bar{w}}{\partial \bar{z}}\right) = -\frac{\partial \bar{P}}{\partial \bar{z}} + \mu_{nf}\left(\frac{\partial^2 \bar{w}}{\partial \bar{r}^2} + \frac{1}{\bar{r}}\frac{\partial \bar{w}}{\partial \bar{r}} + \frac{\partial^2 \bar{w}}{\partial \bar{z}^2}\right) + (\rho\gamma)_{nf} g(\bar{T} - \bar{T}_w) \quad (4)$$

$$(\rho Cp)_{nf}\left(\bar{u}\frac{\partial \bar{T}}{\partial \bar{r}} + \bar{w}\frac{\partial \bar{T}}{\partial \bar{z}}\right) = k_{nf}\left(\frac{\partial^2 \bar{T}}{\partial \bar{r}^2} + \frac{1}{\bar{r}}\frac{\partial \bar{T}}{\partial \bar{r}} + \frac{\partial^2 \bar{T}}{\partial \bar{z}^2}\right) + Q_o \quad (5)$$

where $\rho_{nf}, \mu_{nf}, k_{nf}$ are the density, viscosity, and thermal conductivity of the nanofluid, respectively, γ_{nf} is the thermal expansion coefficient of the nanofluid, and Q_o is the constant of absorption or heat generation parameter. Cp_{nf} is the heat capacitance of the nanofluid.

Standard k − ω Turbulence Model

The two-equation low Re $k-\omega$ turbulent model was incorporated into the Navier-Stokes equation stated above to solve the eddy viscosity that arose due to the transition from laminar to turbulent flow.

The two-equation turbulence model is expressed below:

$k - equation$;

$$\frac{\partial}{\partial t}(\rho k) + \frac{\partial}{\partial \bar{z}}(\rho k \bar{w}) = \frac{\partial}{\partial \bar{r}}\left(\Gamma_k \frac{\partial k}{\partial \bar{r}}\right) + G_k - Y_k \quad (6)$$

$\omega - equation$;

$$\frac{\partial}{\partial t}(\rho \omega) + \frac{\partial}{\partial \bar{z}}(\rho \omega \bar{w}) = \frac{\partial}{\partial \bar{r}}\left(\Gamma_\omega \frac{\partial \omega}{\partial \bar{r}}\right) + G_\omega - Y_\omega \quad (7)$$

where k and ω are turbulence kinetic energy and specific dissipation rate, Γ_k, Γ_ω are effective diffusivity terms, G_k, G_ω are generation terms, Y_k, Y_ω are destruction terms.

$$\Gamma_k = \mu + \alpha^* \left(\rho \frac{k}{\omega}\right) \frac{1}{\sigma_k} \quad (8)$$

$$\Gamma_\omega = \mu + \alpha^* \left(\rho \frac{k}{\omega}\right) \frac{1}{\sigma_\omega} \quad (9)$$

Reynolds number correction factors used to determine the standard variant k-ω turbulence model are as follows;

$$\alpha^* = \alpha_\infty^* \left(\frac{\alpha_0^* + \frac{Re_t}{Re_k}}{1 + \frac{Re_t}{Re_k}}\right), \; G_k = -\rho \bar{u}_i \bar{u}_j \frac{\partial u_j}{\partial x_i}, \quad G_\omega = \alpha \left(\frac{\omega}{k}\right) G_k,$$

$$\alpha = \frac{\alpha_0}{\alpha^*} \left(\frac{\alpha_0 + \frac{Re_t}{Re_\omega}}{1 + \frac{Re_t}{Re_\omega}}\right), \qquad Y_k = \rho \beta^* f_{\beta^*} k\omega, \qquad \beta_i^* = \beta_\infty^* \left[\frac{0.2666 + \left(\frac{Re_t}{R_\beta}\right)^4}{1 + \left(\frac{Re_t}{R_\beta}\right)^4}\right]$$

Closure coefficient for the translational $k-\omega$ turbulent model

$\alpha_\infty^* = 1,\ \alpha_\infty = 0.52,\ \alpha_0 = 0.1111,\ \beta_\infty^* = 0.09.$
$\beta_i = 0.072,\ R_\beta = 8,\ Re_k = 6,\ Re_w = 2.95,\ \xi^* = 1.5$
$M_{t0} = 0.25\ \ \sigma_K = 2.0\ \ \sigma_w = 2.$

C. *Nanofluid thermophysical properties*

The nanofluids used for the studies are Al_2O_3, CuO, SiO_2, and ZnO, the volume fraction of nanoparticles varied from 1.0% to 4.0% (see Table 2). The thermophysical properties of the arterial wall are presented in Table 3. The effective thermophysical properties of the nanofluid are as follows:

Density correlation (Manca *et al*., 2012)

$$\rho_{nf=}(1-\emptyset)\rho_f + \emptyset\rho_{np} \quad (10)$$

Specific heat correlation (Manca *et al.*, 2012)

$$\rho_{nf} Cp_{nf} = (1-\emptyset) Cp_f + \emptyset Cp_{np} \quad (11)$$

Dynamic viscosity

The equation for dynamic viscosity (Masoumi *et al.*, 2009) is employed for the effective viscosity, which is a function of the working fluid and nanofluid physical properties.

$$\mu_{nf} = \mu_f + \frac{\rho_{np} V_B d_{np}^2}{72C\delta} \quad (12)$$

where δ is the boundary layer thickness and V_B is Brownian velocity could be defined below as:

$$V_B = \frac{1}{d_{np}} \sqrt{\frac{18K_c T}{\pi \rho_{np} d_{np}}}, \quad \delta = \sqrt[3]{\frac{\pi}{6\emptyset}} d_{np} \quad (13)$$

$$C = \mu_f{}^{-1}\left[\left(c_1 d_{np} + c_2\right)\emptyset + \left(c_3 d_{np} + c_4\right)\right] \quad (14)$$

where C in Eqn. 14 represents correction factor, c_1, c_2, c_3, and c_4 are experimental coefficients and d_{np} denotes mean diameter of nanoparticles, which is expressed in nanometer:

$c_1 = -0.000001133,\ c_2 = -0.000002771$
$c_3 = 0.00000009,\ c_4 = -0.000000393$ (15)

Thermal conductivity

The equation for thermal conductivity (Hamilton, 1962) is adopted here, where Brownian motion and mean diameter of the nanoparticles are used for estimating the effective thermal conductivity of the nanofluid.

$$k_{nf} = \frac{k_{np} + k_f(\Phi-1) - \emptyset(\Phi-1)(k_f - k_{np})}{k_{np} + k_f(\Phi-1) + \emptyset(k_f - k_{np})} \quad (16)$$

Table 2. The Thermophysical properties for base fluid and nanoparticles at T=300K

Parameter	ρ(kg /m³)	C_p(J/ kgK)	k(W /mk)	μ(Pa.s)
Pure blood	1050	0.549	4390	0.00365
SiO_2	2200	703	1.2	-
Al_2O_3	3970	765	40	-
ZnO	5600	495.2	1.3	-
CuO	6500	535.6	20	-

Table 3. The Thermophysical properties of the arterial wall

Parameter	ρ(kg /m³)	C_p(J/ kgK)	k(W /mk)	μ(Pa.s)
Arterial wall	1075	3490	0.476	-

Table 4. Boundary Condition

Boundary	Location		Condition
Hydrodynamic	Fluid/solid interface		$u = w = 0$
	Inlet at $r=0$,	at $z = 0$	$w = U$,$u=0$ $\frac{\partial w}{\partial r} = 0,\ \frac{\partial u}{\partial r} = 0$
	Arterial wall	at $r = R_i(z)$	(No-slip condition) $u = w = 0$
	Outlet	at $z = L$	$P_{blood=}0$
Thermal	Fluid/Interface		$-k_s\left(\frac{\partial T_s}{\partial n}\right) = -k_f\left(\frac{\partial T_s}{\partial n}\right)$
	Inlet	$at\ z = 0$ $at\ r = 0$	$T_{fblood} = T_f = 310k$ $\frac{\partial T}{\partial r} = 0$
	Arterial wall	$at\ r = R_i(z)$	$T = T_w = 320k$
	Outlet	$at\ z = L$	$-k_f\left(\frac{\partial T_s}{\partial y}\right)0, -k_s\left(\frac{\partial T_s}{\partial y}\right) = 0$
	Turbulence Boundary Condition		
Hydrodynamic	Turbulence intensity		$I = 0.16\left(Re_{nf}\right)^{-\frac{1}{8}}$
	Length scale		$l = 0.07D_h$
	Turbulence viscosity ratio		$\frac{\mu_t}{\mu}$

where Φ denote shape factor and the value of 3 was used in this study (Peyghambarzadeh *et al.*, 2011)

where l_{mf} is a mean-free path of the base fluid and K_c is Boltzmann constant.

$$Re = \frac{\rho_{nf} UD}{\mu_{nf}} \quad (17)$$

$$f = \frac{\nabla PD}{2\rho U^2 l} \quad (18)$$

$$Nu = \frac{zq_c}{k(T_w - T_f)} \quad (19)$$

Nusselt number correlations used for the validation study are listed below;

Dittus-Boelter correlation (Dittus and Boelter, 1985)

$$Nu = 0.023 Re^{0.8} Pr^{0.4} \quad (20)$$

Pak and Cho correlation (Pak and Cho, 2007)

$$Nu = 0.021 Re^{0.8} Pr^{0.5} \quad (21)$$

Maiga *et al*. correlation (Maïga *et al.*, 2005)

$$Nu = 0.085 Re^{0.71} Pr^{0.35} \quad (22)$$

III. NUMERICAL COMPUTATIONS

The Navier-Stokes, energy, and low Reynold k-ω turbulence equations in Eqns. (2)-(9) with the assumptions and boundary conditions in Table 4 are still very complex due to non-linearity. A robust computational commercial code ANSYS (Fluent) software is adopted to solve the complex equations. Here, the finite volume method with a pressure-based solver was used. The software was set for a double-precision and parallel version. The Semi-Implicit Method for Pressure Linked Equation (SIMPLE) algorithm was used for pressure-velocity coupling, and the gauss cell-based was used for the discretization scheme. The second-order scheme was used for pressure, momentum, and energy. The SST k-ω, which was set at low Reynolds, was adopted for the turbulence model, and under-relaxation factors were set for default values, and all equations were set at convergence criteria of 1×10^{-6}.

A. Mesh Generation

The ANSYS meshing was adopted to mesh the geometry of the problem. The vital aspect of this study was to take cognizance as closely as possible of the flow and temperature profile around the stenosis and aneurysm. A structured hexahedral mesh generation technique was created for the geometry (see Figures 4 through 6). It was further subjected to mesh refinement through a high number of divisions at the model edges and elements at the faces to capture the boundary layer flow and thermal field. Finally, the geometry is face meshed to obtain a uniform grid. However, orthogonality, equiangular skewness, and aspect ratio (see Figure 7) were within the acceptable range.

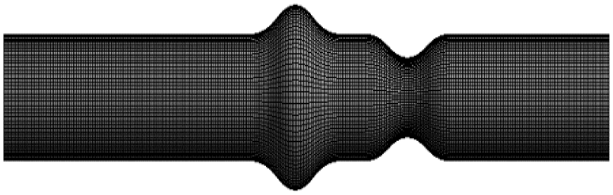

Figure 4. front view of hexahedral structured grids

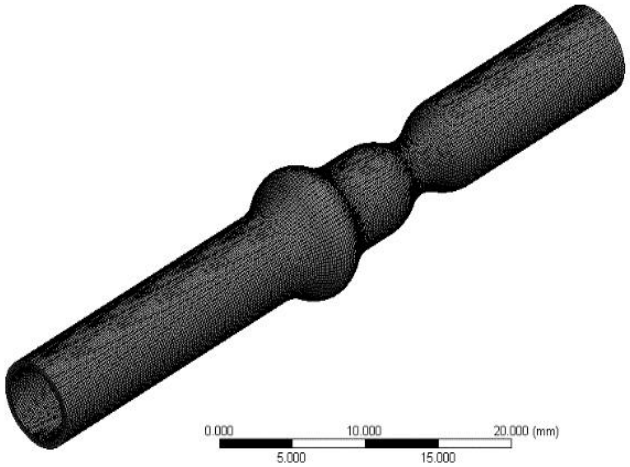

Figure 5. Orthogonal view of the structure grids

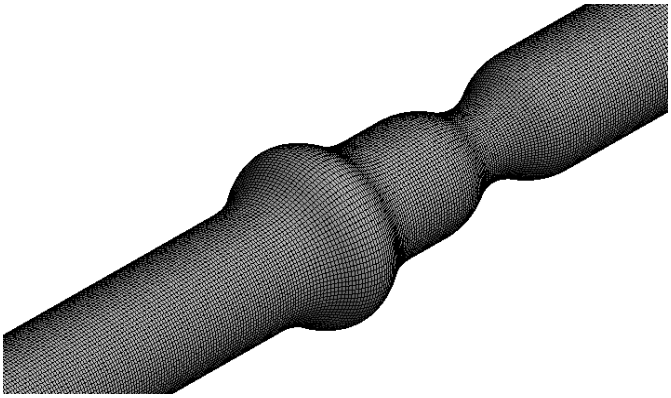

Figure 6. zoom-out view of the mesh

B. Mesh Independence Analysis

Eight different grid sizes (see Table 5) denoted by G1, G2, G3, G4, G5, G6, G7, and G8 are implemented to establish the grid independence of the calculated computational results. Table 5 and Figure 8 show grid sensitivity analysis and compare the Nusselt number at different mesh sizes for the case of SiO_2 at the exit of the artery for nanoparticle concentration of 0%-4%, nanoparticle size of 25nm, and Reynolds number of 500. However, Table 5 and Figure 8 indicate that, the numerical values for the Nusselt number do not significantly alter as the mesh element density is increased above Grid 6. For this numerical investigation, Grid 6 (292994 elements) was chosen.

IV. RESULTS AND DISCUSSION

A. Validation and Verification of Model

To verify and validate the reliability of the numerical model, a comparison is performed between the simulated results of this present study and other experimental results. Similar geometry (circular pipe without constrictions) with that of experimental work of (Pak and Cho, 2007), with Al_2O_3 nanoparticle of size 25nm suspended in water as a based fluid is adopted here for validation. As shown in Figure 9, the Nusselt number results of the present study are well conformed with all the results used for the comparison, mostly in good agreement with the experimental results of (Dittus and Boelter, 1985) and (Pak and Cho, 2007); though less in values compare to numerical results of (Maiga *et al.*, 2005). Therefore, this conformity has shown consistency and accuracy in this numerical model.

B. Effect of nanoparticles on blood velocity

Figure 10 illustrates the effect of the different nanoparticles with a nanoparticle concentration of 4.0% and nanoparticle size of 25nm on the blood flow velocity at a specified location in the diseased coronary artery. As depicted in Figure 10, the addition of nanoparticles to the pure blood causes the fluid velocity to decrease. This is because nanoparticles increased the density of the pure blood, thereby reducing the flow velocity. The SiO_2 nanoparticle has the lowest effect on pure blood velocity compared to other nanoparticles; it reduces flow velocity by 0.65%. Meanwhile, CuO nanoparticles greatly diminish the blood flow velocity by 1.96%. Al_2O_3 and ZnO nanoparticles decreased the blood

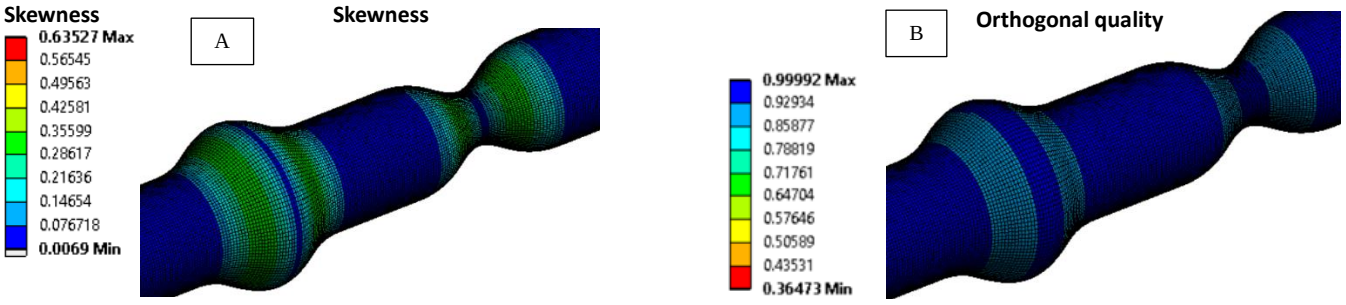

Acceptable range

Maximum skewness < 0.95 Minimum orthogonality > 0.1

Figure 7 (a) Skewness quality of the mesh (b) Orthogonal quality of the mesh

Table 5. Grid Independence Test

Nusselt number for SiO_2 at d_p=25nm

Mesh	Elements	Nodes	Ø=0%	Ø=1%	Ø=2%	Ø=3%	Ø=4%
Grid 8	519515	306001	0.19668	0.20010	0.20186	0.20329	0.20649
Grid 7	405432	292542	0.19668	0.20010	0.20186	0.20329	0.20649
Grid 6	292994	193529	0.19668	0.20010	0.20186	0.20329	0.20649
Grid 5	291229	185123	0.19541	0.19821	0.19913	0.20161	0.20531
Grid 4	287111	174092	0.19384	0.19682	0.19824	0.20004	0.20372
Grid 3	253322	170138	0.19172	0.19522	0.19701	0.19815	0.20258
Grid 2	210418	161709	0.19001	0.19301	0.19520	0.19725	0.20153
Grid 1	201398	112749	0.17405	0.19142	0.19337	0.19585	0.20092

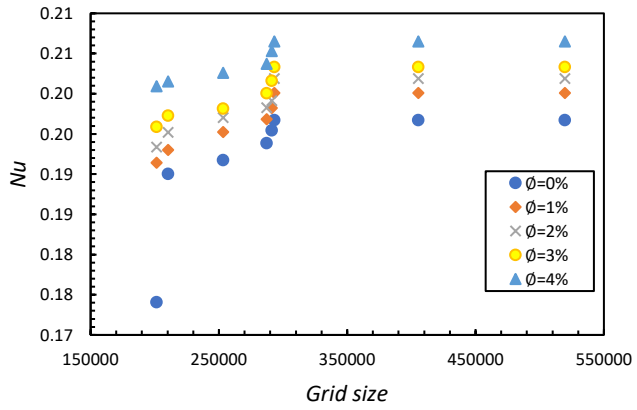

Figure 8. Grid independence test

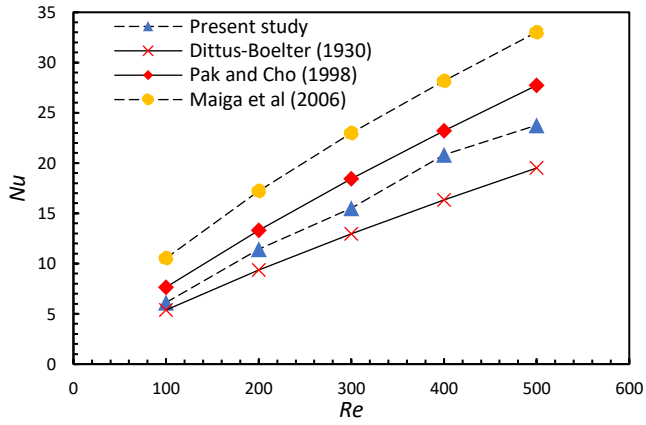

Figure 9. Comparison of numerical results of nanofluid (blood and Al_2O_3) at Ø=4%, d_p=25nm with other experimental results and available correlations

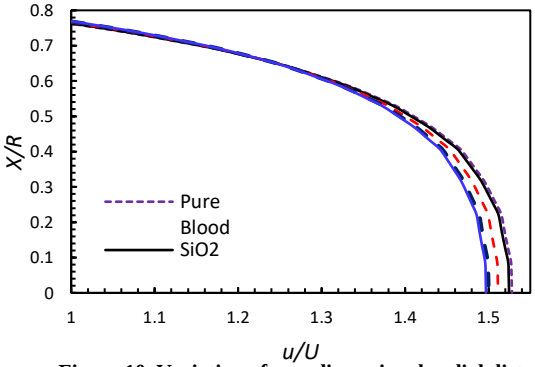

Figure 10. Variation of non-dimensional radial distance against non-dimensional axial velocity for different nanoparticles suspended in a based fluid (blood) at $= 11D$, d_p=25nm and $\emptyset = 4\%$

velocity by 1.31% and 1.63%, respectively. This analysis is not limited to arterial diseases; it may be helpful, especially to the pharmacist, medical doctors, and physicians in treating and managing other diseases.

C. Effect of nanoparticles concentration on blood velocity

Figure 11 shows the influence of nanoparticle concentration on fluid velocity by comparing the different nanoparticle volume fractions (1%-4%) of SiO_2 with a nanoparticle size of 25nm at the exit of the coronary artery on the plot of non-dimensional radial distance against non-dimensional axial velocity. This figure reveals that increasing the nanoparticle concentration decreases the blood velocity at the exit of the coronary artery. The nanofluid viscosity increases as the volume fraction of the nanoparticle is increased. Therefore, obstructs or mitigates the flow velocity. 1.0% increase in the nanoparticle concentration decreases the magnitude of the velocity at the exit of the coronary artery by 0.66%, whereas 2.0%, 3.0%, and 4.0% nanoparticle concentration reduce the velocity of pure blood by 1.3%, 1.34%, and 2.05%, respectively.

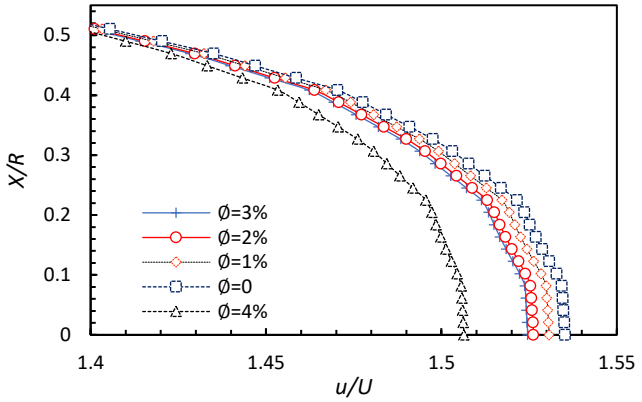

Figure 11. Variation of non-dimensional radial distance against non-dimensional axial velocity for the different volume fraction of SiO_2 in based fluid (blood) at $= 11D$, d_p=25nm

D. Effect of nano-size on blood velocity

Figure 12 demonstrates the impact of different sizes of SiO_2 nanoparticles in the range of 25 nm-100 nm on blood velocity at a specified volume fraction of 4.0%. As shown in Figure 12, by increasing the diameter of the nanoparticle, the nanofluid velocity is reduced because of the reduction in the Brownian forces. Addition of 25 nm of SiO_2 to the base fluid (pure blood) reflect the highest velocity, whereas 100 nanometers of SiO_2 provide the lowest velocity value.

E. Effect of nanoparticle type, concentration, and nanoparticle size on Nusselt number

Figure 13 visualizes the influence of different nanoparticle types (SiO_2, CuO, Al_2O_3, and ZnO) on Nusselt number at a constant volume fraction and nano-size at the specified axial location of the coronary artery within the Reynold number range of 200-500. The results indicate that all nanoparticle types, when added to pure blood, enhance the value of Nusselt number. It is evident that nanofluid containing SiO_2 nanoparticles provides the highest value of the Nusselt number by at most 53% compared to pure blood at *Re* = 500. This is

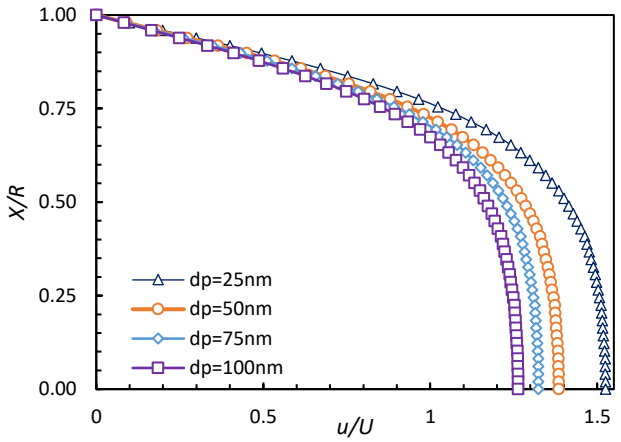

Figure 12. Variation of dimensionless radial distance against dimensionless axial velocity different size of SiO_2 nanoparticles for $\emptyset = 4.0\%$ at $z = 11D$

due to the lowest thermal conductivity of the SiO_2. Among the other nanofluids, a more significant change in Nusselt number is displayed by the SiO_2-pure blood nanofluid. Furthermore, the Nusselt number is a bit lower at the low Reynolds number because of the lower values of the viscosity and high bulk temperature. Meanwhile, at Reynolds number 500, Al_2O_3, ZnO, and CuO nanofluids enhance the Nusselt number of the pure blood by 25.0%, 17.5%, and 8.6%, respectively. Figure 14 reveals the comparison of the Nusselt number against the Reynolds number for SiO_2 nanofluid with a nanoparticle concentration range of 1.0%-4.0% for a constant diameter of the nanoparticles. As shown in Figure 14, for all volume fractions, the Nusselt number sharply increases with the Reynolds number as a result of a significant increase in SiO_2 thermal conductivity and Prandtl number. In addition, the Nusselt number for SiO_2-pure blood nanofluid steeply increases with an increase in nanoparticle volume fraction. At *Re*=500, it is revealed that a 4.0% volume fraction of SiO_2 nanoparticles in the pure blood could elevate the Nusselt number of the based fluid by 3.7%. Figure 15 shows the effect of different SiO_2 nanoparticles (25nm-100nm) on Nusselt number with a volume fraction of 4.0% at the exit of the coronary artery consisting of both stenosis and aneurysm. For any given size of the nanoparticle, the Nusselt number increases with the Reynolds number. However, reducing the size of the nanoparticle increases the Nusselt number because Brownian motion becomes more aggravated at the smaller size of the nanoparticles, which in turn increases the thermal conductivity. At *Re*=500, the 25nm size of SiO_2 with 4.0% volume fracture in pure blood increases the Nusselt number by 32% compared to the 100nm diameter of the nanoparticles.

F. Effect of nanoparticle type, concentration, and nanoparticle size on the temperature profile

Figure 16 presents the radial temperature profile of different nanoparticle types in pure blood at z=11D for Re=500, $\emptyset = 4.0\%$ and $d_p = 25$ nm. This Figure reveals that the temperature profile for all the nanofluids is in parabolic form; at $0 \leq x/R \leq 0.2$, it remains flat or constant, i.e., no significant change in the temperature profile of the nanofluid

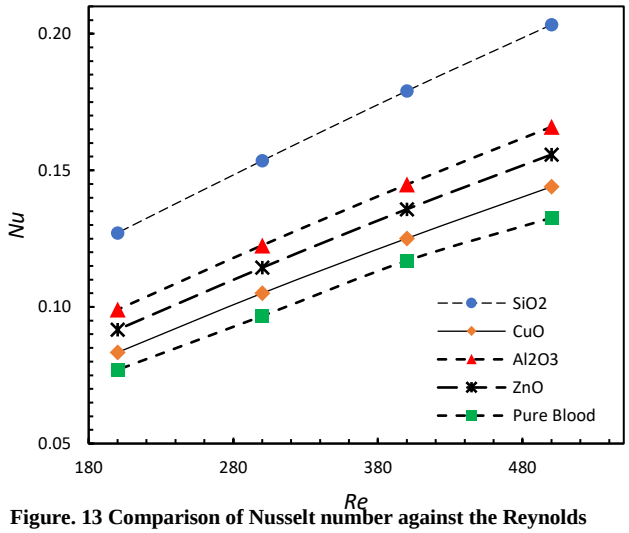

Figure. 13 Comparison of Nusselt number against the Reynolds number at different nanoparticles at $\emptyset = 4\%$, $d_p = 25nm$ and $z = 11D$

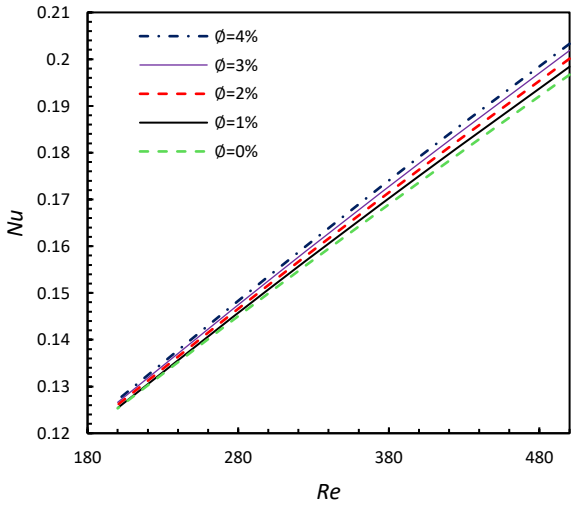

Figure 14. Comparison of Nusselt number against the Reynolds number for SiO_2 at different volume fractions at $d_p = 25nm$ and $z = 11D$

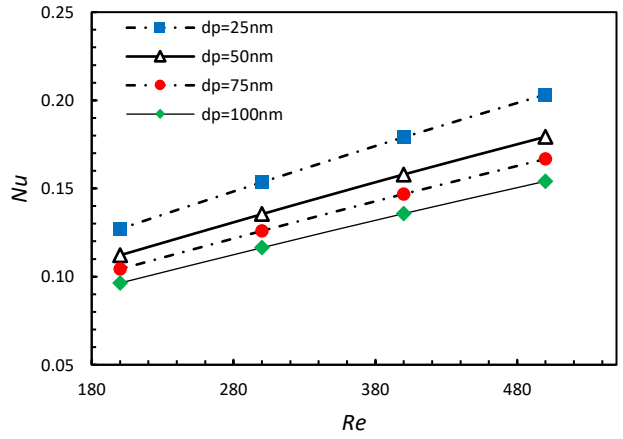

Figure 15. Comparison of the Nusselt number against the Reynolds number for SiO_2 at a different diameter of nanoparticle at $\emptyset = 4.0\%$ and $z = 11D$

at the core of the coronary artery. At $0.2 \leq x/R \leq 0.6$, the temperature gradually increases with radial distance, whereas at $0.6 \leq x/R \leq 1$, a steep increase in temperature profile is evident. The highest temperature is seen at the arterial wall for all cases of the nanofluids. Here, nanoparticles increase the thermal conductivity of pure blood; Al_2O_3-pure blood nanofluid provides the highest value of temperature, followed by CuO, ZnO, and SiO_2. This is due to its more significant thermal conductivity than other nanoparticle types. Figure 17 illustrates the effect of volume fraction (0%-4%) on the temperature profile; for all cases of volume fraction, the temperature increases with radial distance. The temperature at the exit is enhanced by increasing the volume fraction of the nanoparticle. At the core of the artery, a 4% volume fraction of SiO_2 in pure blood increases the temperature by approximately 2%. Figure 18 indicates the effect of nanoparticle diameter on temperature. The results show that temperature increases by increasing the nanoparticle's diameter or size. 100 nm of SiO_2 in pure blood depicts the highest temperature value, and 25 nm gives the lowest temperature value.

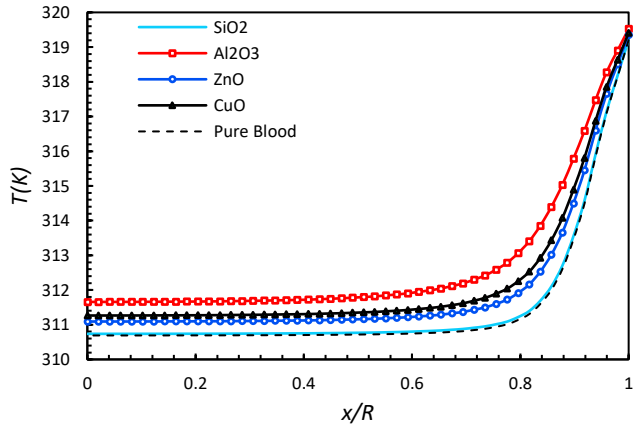

Figure 16. Effect of different nanoparticle types on the radial temperature at $z = 11D$ for Re =500, $\emptyset = 4.0\%$ and $d_p = 25nm$.

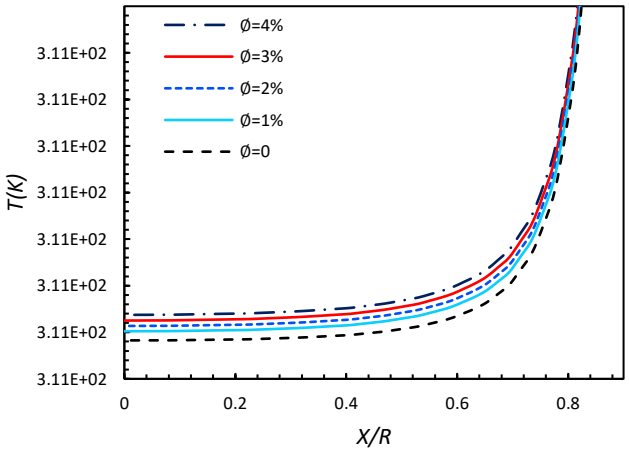

Figure 17. Effect of different volume fractions on radial temperature for SiO_2 at $z = 11D$, $Re = 500$ and $d_p = 25nm$

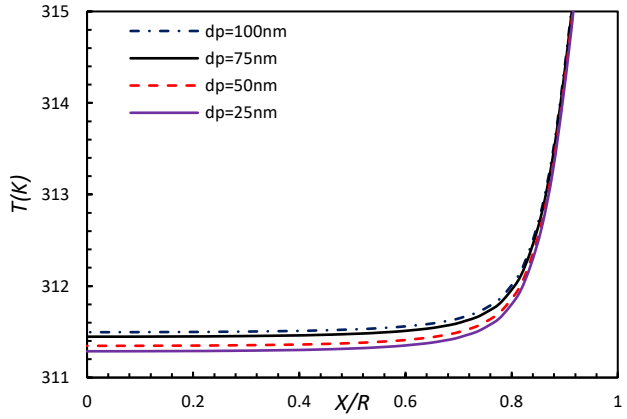

Figure 18. Effect of different nanoparticle diameters on radial temperature for SiO_2 at $z = 11D$, $Re = 500$, and $\emptyset = 4.0\%$

G. Effect of Nanoparticle type, concentration, and nanoparticle size on skin friction coefficient

Figure 19 illustrates the influence of nanoparticles of different types on skin friction coefficient at the exit of the coronary artery for $\emptyset = 4.0\%$ and $d_p = 25nm$. As seen from Figure 19, the skin friction coefficient decreases with a rise in Reynolds number for all cases of nanoparticle type. The impact of nanoparticle type on the skin friction coefficient of pure blood is evident. SiO_2-pure blood nanofluid has the highest value of skin friction coefficient of about 0.007676, and the lowest value of exactly 0.006763 is reported in CuO-pure blood nanofluid. This is because SiO_2 nanoparticles have the least density compared to other nanoparticles. Figure 20 indicates the effect of nanoparticle volume fraction on the skin friction coefficient. As clearly depicted in Figure 20, increasing the concentration of nanoparticles (1%-4%) in the pure blood does not reflect any significant change in the skin friction coefficient. Figure 21 reveals that no significant change in skin friction coefficient is observed for all cases of nanoparticle sizes (25 nm-100 nm).

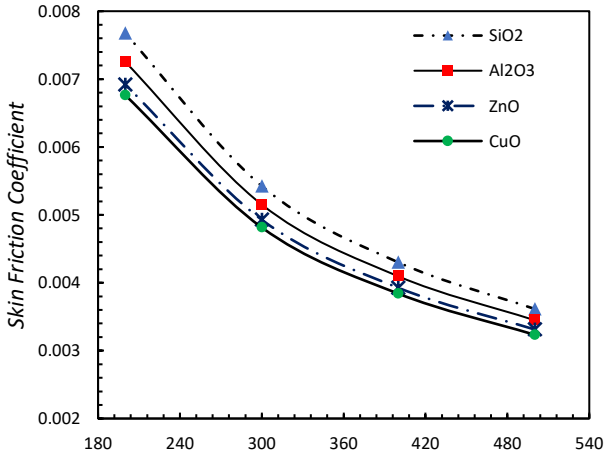

Figure 19. Variation of skin friction coefficient against Reynolds number for different nanoparticle types at z=11D, $\emptyset = 4\%$ and $d_p = 25nm$.

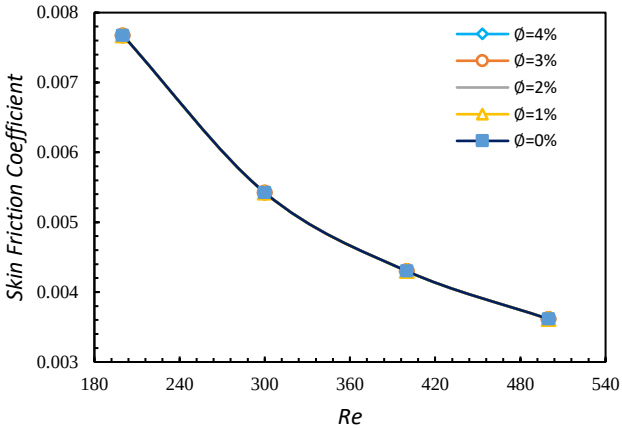

Figure. 20 Variation of skin friction coefficient against Reynolds number for different volume fractions for SiO_2-Pure blood nanofluid at z=11D, and $d_p = 25nm$

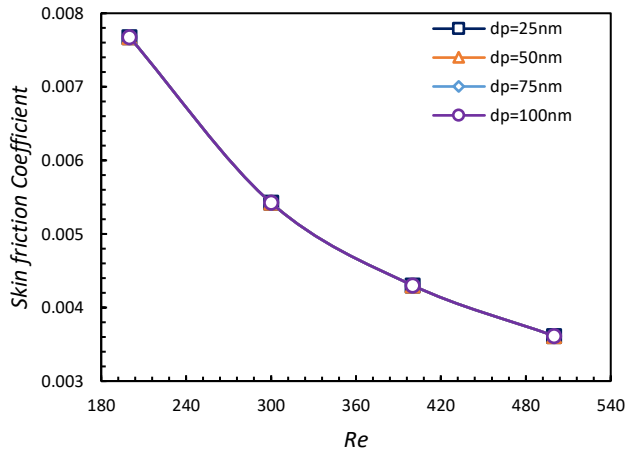

Figure 21. Variation of skin friction coefficient against Reynolds number for different nanoparticle diameters for SiO_2-Pure blood nanofluid at z=11D

H. Temperature contour

Figure 22 reveals the temperature distribution in a diseased artery for different nanoparticle types. As can be seen in the contour plot, the presence of an aneurysm and stenosis in the coronary artery causes a huge distortion in the temperature distribution. It is also observed that the temperature at or near the artery's wall is higher than at the center. The probe tool in the CFD post-processing section of ANSYS was used to take the temperature in the vicinity of the aneurysm and stenosis. It was noticed that an increased temperature magnitude is seen in the vicinity of the aneurysm. In contrast, a decreased temperature is reported in the region of the stenosis for all cases of the nanoparticle type.

I. Turbulence Intensity contour

Figure 23 displays the flow disturbance of the SiO_2-blood nanofluid in the artery with a combination of aneurysm and stenosis with varied volume fractions at a Re=500 and $d_p = 25nm$. It is indicated in the figures that for all cases of volume fractions, turbulence intensity is greatest at the proximity of the

stenosis and decreases outwardly downstream of the stenosis. The turbulence intensity increases as the volume fraction is increased.

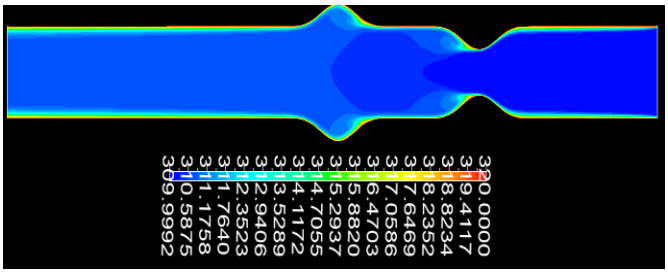

(a)

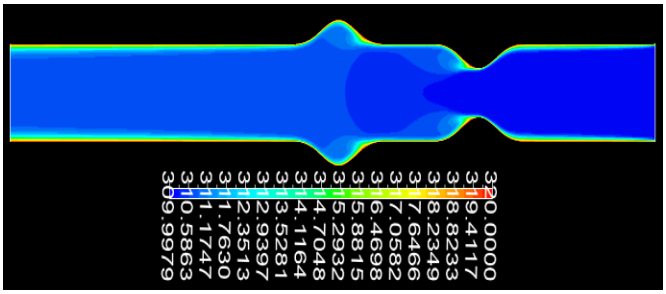

(b)

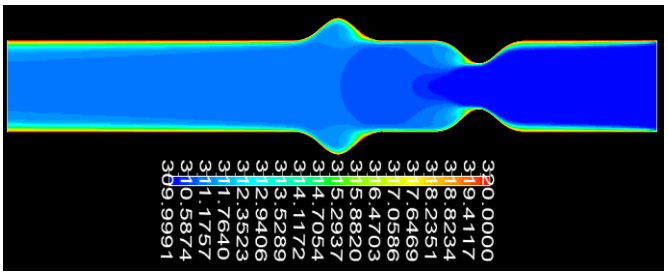

(c)

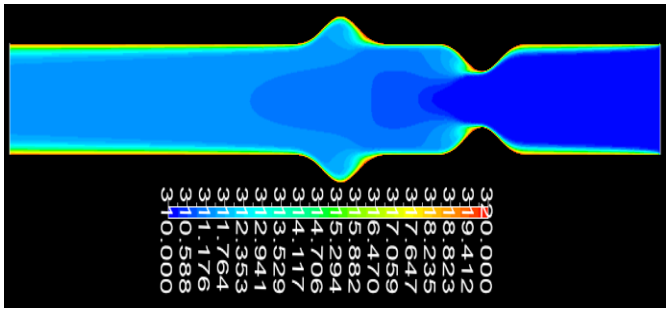

(d)

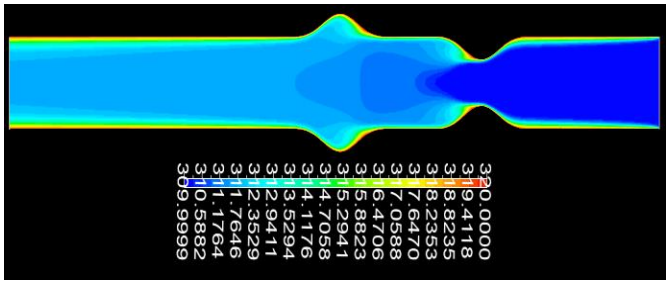

(e)

Figure 22. Temperature Contour for (a) Pure Blood (b) SiO_2+Pure blood (c) ZnO+Pure blood (d) CuO + Pure blood (e) Al_2O_3+Pure blood for $\emptyset = 4.0\%$, $d_p = 25nm$ and $Re = 500$.

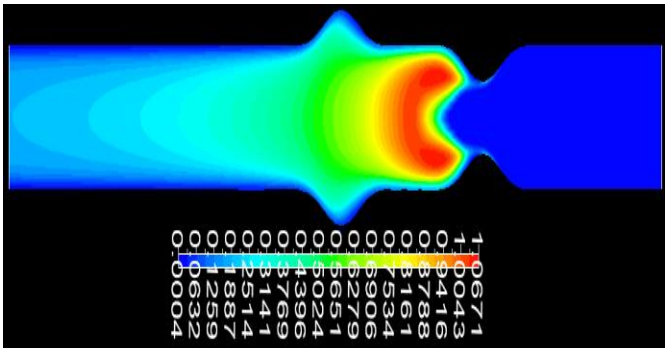

(a)

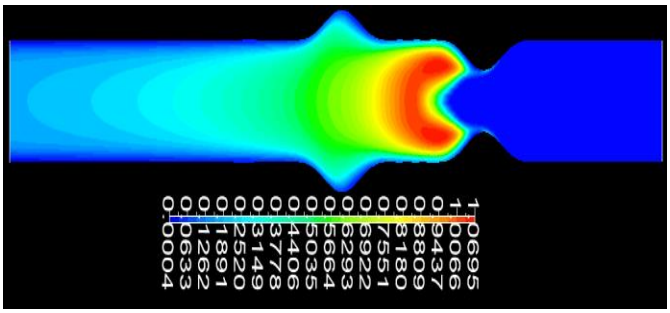

(b)

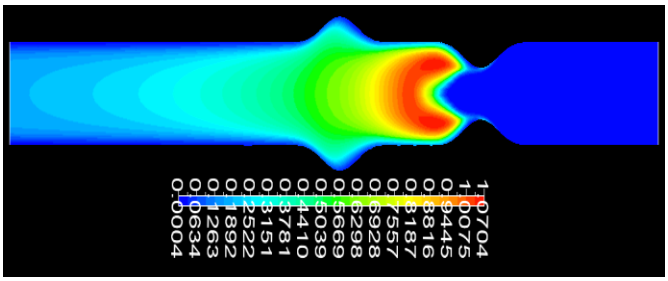

(c)

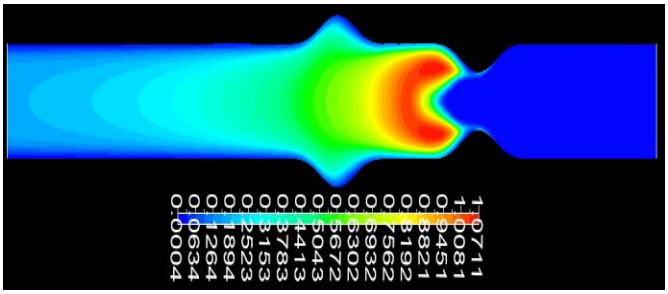

(d)

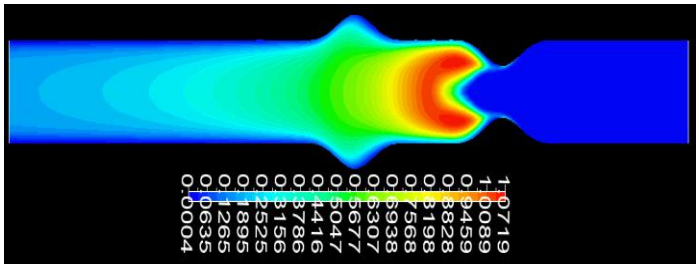

(e)

Figure 23. Turbulence intensity contour for SiO_2+Pure blood nanofluid, at $d_p = 25nm, Re = 500$ for different volume fractions (a) $\emptyset = 0$ (Pure Blood) (b) $\emptyset = 1\%$ (c) $\emptyset = 2\%$ (d) $\emptyset = 3\%$ (e) $\emptyset = 4\%$

V. CONCLUSION

A computational study has been performed to investigate the effects of nano-pharmacological particles on the blood flowing through the diseased coronary artery. This study is aimed at simulating nanoparticle drug delivery in the treatment of hemodynamic ailments. The key findings from the computational simulations can be summarized as follows:

1) The suspension of 4% volume fraction of CuO, Al_2O_3, ZnO and SiO_2 nanoparticles to the blood reduced the flow velocity by 1.96%, 1.31%, 1.63 and 0.65%, respectively.
2) Increasing the nanoparticles concentration from 1% to 4% reduced the flow velocity by 0.66% to 2.05%.
3) At a fixed volume fraction of 4% and Re of 500, addition of SiO_2, CuO, Al_2O_3, and ZnO nanoparticles to the blood reduced the Nu by 53%, 25%, 17.5%, and 8.6%, respectively.

   The highest and lowest value of skin friction factor was observed in SiO_2 and CuO nanofluid, respectively.

AUTHOR CONTRIBUTIONS

I. A. Fetuga: Conceptualization, Software, Validation, Writing–original draft, Data curation. **O. O. Olakoyejo:** Supervision, Writing review and Editing, Resources, Validation, Project Adminstration. **O. Oluwatusin:** Supervision, Project Adminstration, Resources. **O. A. Adelaja:** Supervision, Validation, Project Adminstration. **J.K. Gbegudu:** Methodology, Formal analysis. **K. S. Aderemi:** Methodology, Data curation, Literature review. **E. A. Adeyemi:** Writing – review & editing, Literature review.

REFERENCES

El Bécaye Maïga, S.; S.J. Palm; C.T. Nguyen; G. Roy and N. Galanis. (2005). Heat transfer enhancement by using nanofluids in forced convection flows. International Journal of Heat and Fluid Flow, 26(4): 530-546. doi: 10.1016/j.ijheatfluidflow.2005.02.004.

Bluestein, D.; L. Niu; R.T. Schoephoerster and M.K. Dewanjee. (1996). Steady Flow in an Aneurysm Model: Correlation Between Fluid Dynamics and Blood Platelet Deposition. Journal of Biomechanical Engineering, 118(3): 280–286. doi: 10.1115/1.2796008.

Casson, N. (1959). A Flow Equation for Pigment-Oil Suspensions of the Printing Ink Type. Rheology of disperse systems, 84–102.

Choi, S. U.S.; Z.G. Zhang; W. Yu; F.E. Lockwood and E.A. Grulke. (2001). Anomalous thermal conductivity enhancement in nanotube suspensions. Applied Physics Letters, 79(14): 2252. doi: 10.1063/1.1408272.

Choi, S. U. S.; S. Li and J. A. Eastman. (1999). Measuring Thermal Conductivity of Fluids Containing Oxide Nanoparticles. Journal of Heat Transfer, 121(2): 280–289. doi: 10.1115/1.2825978.

Dittus, F.W. and Boelter, L.M.K. (1985). Heat transfer in automobile radiators of the tubular type. International communications in heat and mass transfer, 12(1): 3–22.

Ellahi, R.; S.U. Rahman.; S. Nadeem and N.S. Akbar. (2014). Blood flow of nanofluid through an artery with composite stenosis and permeable walls. Applied Nanoscience (Switzerland), 4(8): 919–926. doi: 10.1007/S13204-013-0253-6/FIGURES/17.

Frank-Ito, D. O. and Cohen, S. M. (2021). Orally Inhaled Drug Particle Transport in Computerized Models of Laryngotracheal Stenosis. Otolaryngology–Head and Neck Surgery, 164(4): 829–840. doi: 10.1177/0194599820959674.

Gosman, R. E.; R. M. Sicard; S. M. Cohen. and D. O. Frank-Ito. (2022). Comparison of Inhaled Drug Delivery in Patients With One- and Two-level Laryngotracheal Stenosis. The Laryngoscope, 133(2): 366-374. doi: 10.1002/LARY.30212.

Hamilton, R. L. (1962). Thermal conductivity of heterogeneous two-component systems. Industrial and Engineering Chemistry Fundamentals, 1(3): 187–191. doi: 10.1021/I160003A005/ASSET/I160003A005.FP.PNG_V03.

Karimi, M.; H. Zare; A. Bakhshian; N. Yazdani; M. Hamrang; E. Mohamed; P.S. Zangabad; S. Masoud; M. Basri; L. Bakhtiari and M.R. Hamblin. (2016). Nanotechnology in diagnosis and treatment of coronary artery disease. Nanomedicine, 11(5): 513–530. doi: 10.2217/NNM.16.3.

Karimi, S.; M. Dadvar; M. Dabagh; P. Jalali; H. Modarress and B. Dabir. (2013). Simulation of pulsatile blood flow through stenotic artery considering different blood rheologies: comparison of 3d and 2d-axisymmetric models. Biomedical Engineering: Application, Basis and Communications, 25(2): 1350023. doi: 10.4015/S1016237213500233.

Keith, L.; A. Moore and A.M.R. Agur. (2009). Clinically Oriented Anatomy. Lippincott Williams & Wilkins.

Kent, K. C. (2014). Clinical practice: Abdominal aortic aneurysms. The New England journal of medicine, 371(22): 2101–8. doi: doi: 10.1056/nejmcp1401430/suppl_file/nejmcp1401430_disclosures.pdf..

Manca, O.; S. Nardini; D. Ricci and S. Tamburrino. (2012). Numerical investigation on mixed convection in triangular cross-section ducts with nanofluids, Advances in Mechanical Engineering, 4: 139370. doi: 10.1155/2012/139370.

Mandal, D. K.; P. Goswami; N. Biswas and N. K. Manna. (2022). Fluid Mechanics in Arterial Diseases: Computational Study. In Advances in Computational Approaches in Biomechanics, 153-178. IGI Global. doi: 10.4018/978-1-7998-9078-2.CH010.

Masoumi, N.; N. Sohrabi and A. Behzadmehr. (2009). A new model for calculating the effective viscosity of nanofluids. Journal of Physics D: Applied Physics, 42(5): 055501. doi: 10.1088/0022-3727/42/5/055501.

Masuda H.; A. Ebata and K. Termae (1993). Alteration Of Thermal Conductivity And Viscosity Of Liquid By Dispersing Ultra-Fine Particles. Dispersion of Al_2O_3, SiO_2 and TiO_2 Ultra-Fine Particles. 7(4): 227–233.

Mekheimer, K. S.; M. H. Haroun and M. A. El Kot. (2011). Induced magnetic field influences on blood flow through an anisotropically tapered elastic artery with overlapping stenosis in an annulus. Canadian Journal of Physic, 89(2): 201–12. doi: 10.1139/P10-103.

Nadeem, S. and Ijaz, S. (2015). Theoretical analysis of metallic nanoparticles on blood flow through stenosed artery with permeable walls. Physics Letters A, 379(6): 542–554. doi: 10.1016/J.PHYSLETA.2014.12.013.

Pak, B. C. and Cho, Y. I. (2007). Hydrodynamic and heat transfer study of dispersed fluids with submicron metallic oxide particles. Experimental Heat Transfer, 11(2): 151–170. doi: 10.1080/08916159808946559.

Peyghambarzadeh, S. M.; S. H. Hashemabadi; S. M. Hoseini and J. M. Seifi (2011). Experimental study of heat transfer enhancement using water/ethylene glycol based nanofluids as a new coolant for car radiators. International Communications in Heat and Mass Transfer, 38(9): 1283–1290. doi: 10.1016/j.icheatmasstransfer.2011.07.001

Pincombe, B. and Mazumdar, J. (1997). The effects of post-stenotic dilatations on the flow of a blood analogue through stenosed coronary arteries. Mathematical and Computer Modelling, 25(6): 57–70. doi: 10.1016/S0895-7177(97)00039-3.

Rhee, J. W. and Wu, J. C. (2013). Advances in nanotechnology for the management of coronary artery disease, Trends in Cardiovascular Medicine, 23(2): 39–45. doi: 10.1016/J.TCM.2012.08.009.

Smith, F. T. (1979). The separating flow through a severely constricted symmetric tube. Journal of Fluid Mechanics, 90(4): 725–754. doi: 10.1017/S0022112079002500

Ul Haq, U.; A. Ahmed; Z. Mustansar; A. Shaukat; S. Cukovic; F. Nadeem and L. Margetts. (2022). Computational modeling and simulation of stenosis of the cerebral aqueduct due to brain tumor. Engineering Applications of Computational Fluid Mechanics, 16(1): 1018-1030. doi: 10.1080/19942060.2022.2056511.

Waqas, H.; U. Farooq; D. Liu; M. Alghamdi; S. Noreen and T. Muhammad. (2022). Numerical investigation of nanofluid flow with gold and silver nanoparticles injected inside a stenotic artery. Materials & Design, 223: 111130. doi: 10.1016/J.MATDES.2022.111130.

Yi, J.; F. B. Tian; A. Simmons and T. Barber (2022). Impact of Modelling Surface Roughness in an Arterial Stenosis. Fluids, 7(5): 179. doi: 10.3390/FLUIDS7050179.